JOURNAL OF APPLIED ELECTROCHEMISTRY 4 (1974) 191–200

Thermodynamic diagrams of the copper/molten potassium nitrate system

S. L. MARCHIANO and A. J. ARVIA

INIFTA, División Electroquimica, Facultad de Ciencias Exactas, Universidad Nacional de La Plata, La Plata, Argentina

Received 13 November 1973

Thermodynamic diagrams for the copper/molten potassium nitrate system have been calculated and expressed either as potential/pO^{2-}, potential/pO_2^- or potential/pO_2^{2-} diagrams. They exhibit the corresponding immunity, active dissolution, passivity and transpassivity regions.

1. Introduction

Thermodynamic diagrams of different metal/molten alkaline nitrate systems have been calculated on the basis of the Lux-Flood acid-base theory applied to molten nitrates, on the assumption that the following equilibrium occurs:

$$NO_3^- = NO_2^+ + O^{2-} \qquad (1)$$

This equilibrium involves the existence of O^{2-} and NO_2^+ ions together with NO_3^- ion as the main ionic species in the nitrate melts [1]. The application of E/pO_2 diagrams to the interpretation of metal corrosion in nitrate melts has already been discussed [2–4]. Nevertheless, according to recent electrochemical investigations there is no clear evidence of equilibrium (Equation 1) in these melts, so that instead of those ionic species the occurrence of other ions, such as O_2^- and O_2^{2-}, have been determined [5–7].

The concentrations of the various oxygen ionic species in the alkaline nitrate melts decrease in the order $[O_2^-] > [O_2^{2-}] > [O^{2-}]$. This fact suggested a different approach to calculate the thermodynamic diagrams of metal/molten nitrate systems, based upon O_2^- and O_2^{2-} ions as electroactive species instead of the O^{2-} ion. These calculations are reported in the present paper with reference to the copper/molten potassium nitrate system at different temperatures. The three potential/(log concentration)$^{-1}$ plots define areas of immunity, corrosion and passivity which will be compared with experimental data derived from voltammetric runs made with the copper/molten alkaline nitrate system [7]. Preliminary results on the electrochemical behaviour of this system at 250°C indicate film formation on the copper surface mainly consisting of Cu_2O [8].

2. Results

2.1. *The potential/pO^{2-} diagram*

The calculation procedure to obtain the potential/pO^{2-} diagram of the copper/potassium nitrate melt in the 500–700 K range, is the same as that already described in previous publications [2–4, 9]. The potentials are referred to the standard nitrate reversible electrode which corresponds to the following equilibrium:

$$NO_3^-(l) = NO_2(g) + \tfrac{1}{2}O_2(g) + e. \qquad (2)$$

Most of the thermal data were taken from the literature [10–12], and when the energies of formation were not available, they were estimated through the corresponding Born-Haber cycle. Thus, the standard free energies of formation of $CuNO_3$ and $Cu(NO_3)_2$ were evaluated respectively from the following equilibria:

$$KNO_3(l) + CuCl(s) = KCl(s) + CuNO_3(s) \quad (3)$$

Table 1.

No.	*Reaction*	*Nernst equation*	ΔG°_{500}	E°_{500}	ΔG°_{600}	E°_{600}	ΔG°_{700}	E°_{700}
1	$Cu^+ + 1e = Cu$	$E = E^\circ + \frac{RT}{F} \ln [Cu^+]$	26·592	−1·153	21·861	−0·950	17·740	−0·769
2	$Cu^{2+} + 2e = Cu$	$E = E^\circ + \frac{RT}{2F} \ln [Cu^{2+}]$	35·418	−0·768	25·371	−0·550	16·461	−0·357
3	$Cu^{2+} + 1e = Cu^+$	$E = E^\circ + \frac{RT}{F} \ln \frac{[Cu^{2+}]}{[Cu^+]}$	8·826	−0·383	3·510	−0·152	−1·279	+0·055
4	$Cu_2O + 2e = 2Cu + O^{2-}$	$E = E^\circ + \frac{RT}{2F} pO^{2-}$	122·551	−2·656	111·368	−2·414	102·668	−2·225
5	$CuO + 2e = Cu + O^{2-}$	$E = E^\circ + \frac{RT}{2F} pO^{2-}$	116·931	−2·535	105·123	−2·279	95·849	−2·078
6	$2CuO + 2e = Cu_2O + O^{2-}$	$E = E^\circ + \frac{RT}{2F} pO^{2-}$	111·311	−2·413	98·878	−2·143	89·030	−1·930
7	$CuO + 1e = Cu^+ + O^{2-}$	$E = E^\circ - \frac{RT}{F} \ln [Cu^+] + \frac{RT}{F} pO^{2-}$	90·339	−3·916	83·262	−3·610	78·109	−3·386
8	$\frac{1}{2}O_2 + 2e = O^{2-}$	$E = E^\circ + \frac{RT}{2F} \ln P_{O_2}^{1/2} + \frac{RT}{2F} pO^{2-}$	90·779	−1·968	81·080	−1·757	73·873	−1·60
9	$2Cu^+ + O^{2-} = Cu_2O$	$pO^{2-} = \frac{-(\Delta G^\circ - 2RT \ln [Cu^+])}{RT}$	−69·367	$pO^{2-} = 30·42$	−67·676	$pO^{2-} = 24·72$	−67·188	$pO^{2-} = 21·05$
10	$Cu^{2+} + O^{2-} = CuO$	$pO^{2-} = \frac{-(\Delta G^\circ - RT \ln [Cu^{2+}])}{RT}$	−81·513	$pO^{2-} = 35·75$	−79·752	$pO^{2-} = 29·15$	−79·338	$pO^{2-} = 24·87$

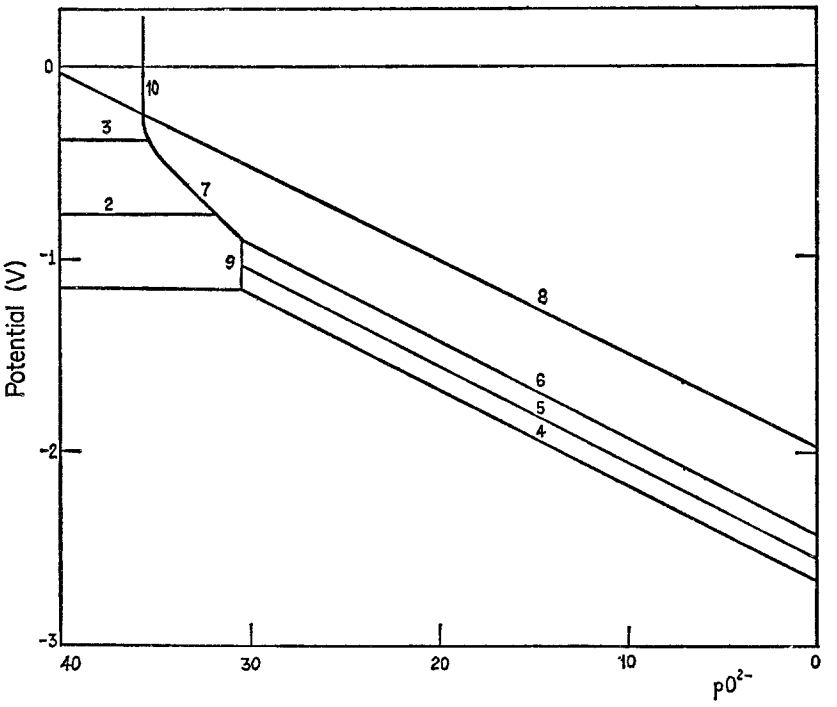

Fig. 1. Potential/pO^{2-} diagram at 500K. The numbers correspond to the equilibria shown in Table 1.

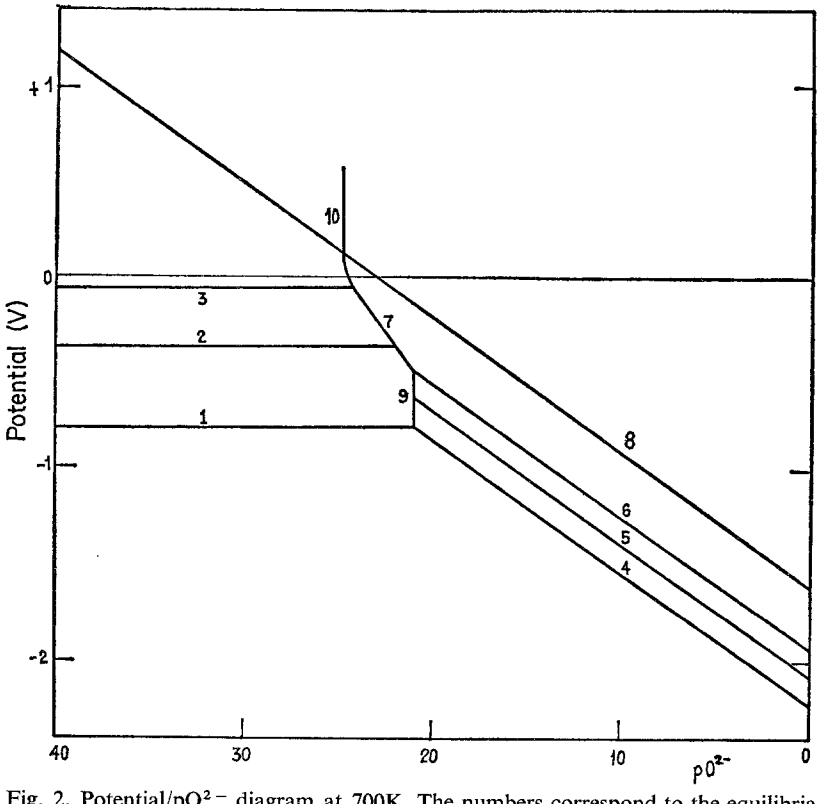

Fig. 2. Potential/pO^{2-} diagram at 700K. The numbers correspond to the equilibria shown in Table 1.

and

$$2KNO_3(l)+CuCl_2(s) = 2KCl(s)+Cu(NO_3)_2(s). \quad (4)$$

Table 1 contains the various equilibria involving copper, copper ions, copper oxides and oxygen which were considered to evaluate the potential/pO^{2-} diagrams shown in Figs. 1 and 2. The corresponding Nernst equations, standard free energies of formation and standard potentials at 500, 600 and 700 K are also assembled in Table 1.

2.2. *The potential/pO_2^- and potential/pO_2^{2-} diagrams*

Recent electrochemical studies on molten alkaline nitrates either pure or with the addition of sodium oxide [6, 7, 13], indicate the existence of the following equilibria involving NO_2^- and O_2^{2-} ions:

$$O^{2-}+NO_3^- = O_2^{2-}+NO_2^- \quad (5)$$

and

$$O_2^{2-}+2NO_3^- = 2NO_2^-+2O_2^- \quad (6)$$

The different oxygen ions are involved in electron transfer and disproportionation reactions [6]:

$$O_2+2e = O_2^- \quad (7)$$

$$O_2^-+e = O_2^{2-} \quad (8)$$

and

$$2O_2^- = O_2^{2-}+O_2. \quad (9)$$

The concentrations of the different oxygen ionic species are related by the disproportionation constant,

$$K_9 = \frac{[O_2][O_2^{2-}]}{[O_2^-]^2} = (3{\cdot}5\pm1)\times10^{-6} \text{ at } 229°C,$$

and by the equilibrium constant,

$$K_5 = \frac{[NO_2^-][O_2^{2-}]}{[NO_3^-][O^{2-}]} = 3 \text{ at } 229°C \text{ [6]}.$$

The values of the equilibrium constant make it clear that the important oxygen anions in the nitrate melts are the superoxide (O_2^-) and the peroxide (O_2^{2-}) ions rather than the oxide (O^{2-}) ion. In the presence of oxygen at appreciable partial pressures any oxide or peroxide is converted virtually completely to superoxide. These equilibria apparently determine the high oxidizing power of the molten alkaline nitrates as compared to other oxoanion-containing melts.

The ratio of the concentrations of the different oxygen ionic species depends on the ionic composition of the melt and on the amount of dissolved oxygen. The alkaline oxides are rather insoluble in the nitrate melt, the dissolution apparently occurring by a chemical reaction through O_2^{2-} and O_2^- ion formation [13]. At 500K and a pO^{2-} of about 18, the O_2^- ion concentration is of the order of 10^{-5} mol per 1000 g and it increases slightly with the amount of sodium oxide present in the melt [14]. When sodium oxide exists in the nitrate melt, the NO_2^- ion concentration is comparable to the O_2^- ion concentration at equilibrium, and the O^{2-} and O_2^{2-} ion concentrations are various orders of magnitude lower than the O_2^- ion concentration. The O^{2-} and O_2^{2-} ion concentrations increase rapidly when the amount of sodium oxide added is increased in the absence of oxygen. On the basis of Equations 5 to 9 the thermodynamic diagram can be presented in terms of either pO_2^- or pO_2^{2-}, assuming the O_2^- and O_2^{2-} ions are respectively, the potential-determining species.

Since no thermal data related to species containing O_2^- and O_2^{2-} ions are available, the estimated standard potentials of the redox couples of Equations 7 and 8 reported in the literature were used directly. These standard potentials were calculated from the corresponding half-wave potentials neglecting the terms containing the activity and diffusion coefficient ratio in the Nernst equations. The half-wave potentials were obtained from voltammogrammes run with platinum electrodes and $NaNO_3$-KNO_3 eutectic at 229°C [6]. This procedure implies an error in the standard potentials of about 10 mV [6]. Table 2 contains the Nernst equations, standard free energies of formation and standard potentials at 500K, calculated for the different reactions which were considered to evaluate the potential/pO_2^- diagram shown in Fig. 3. To calculate equilibria where the NO_2^- ion is involved, the standard free energy change of the reaction:

$$NO_2^-(l) = NO_2(g)+e \quad (10)$$

Table 2.

No.	*Reaction*	*Nernst equation*	ΔG°_{500}	E°_{500}
1	$Cu^+ + 1e = Cu$	$E = E^\circ + \frac{RT}{F} \ln [Cu^+]$	26·592	−1·153
2	$Cu^{2+} + 2e = Cu$	$E = E^\circ + \frac{RT}{2F} \ln [Cu^{2+}]$	35·418	−0·768
3	$Cu^{2+} + e = Cu^+$	$E = E^\circ + \frac{RT}{F} \ln \frac{[Cu^{2+}]}{[Cu^+]}$	8·826	−0·383
4	$2Cu_2O + 1e = 4Cu + O^{=}$	$E = E^\circ + \frac{RT}{F} pO^{=}$	91·985	−3·987
5	$2CuO + 1e = 2Cu + O^{=}$	$E = E^\circ + \frac{RT}{F} pO^{=}$	80·745	−3·50
6	$4CuO + 1e = 2Cu_2O + O^{=}$	$E = E^\circ + \frac{RT}{F} pO^{=}$	69·505	−3·01
7	$4Cu^+ + O^{=} + 3e = 2Cu_2O$	$E = E^\circ + \frac{RT}{3F} \ln [Cu^+]^4 - \frac{RT}{3F} pO^{=}$	14·383	−0·208
8	$2Cu^+ + O^{=} + 1e = 2CuO$	$E = E^\circ + \frac{RT}{F} \ln [Cu^+]^2 - \frac{RT}{F} pO^{=}$	−27·561	1·195
9	$2Cu^{2+} + O^{=} + 3e = 2CuO$	$E = E^\circ + \frac{RT}{3F} \ln [Cu^{2+}]^2 - \frac{RT}{3F} pO^{=}$	−9·909	0·143
10	$4Cu^{2+} + O^{=} + 7e = 2Cu_2O$	$E = E^\circ + \frac{RT}{7F} \ln [Cu^{2+}]^4 - \frac{RT}{7F} pO^{=}$	49·687	−0·308
11	$2Cu + 2Cu^+ + O^{=} + 1e = 2Cu_2O$	$E = E^\circ + \frac{RT}{F} \ln [Cu^+]^2 - \frac{RT}{F} pO^{=}$	−38·801	1·682
12	$O_2 + 1e = O^{=}$	$E = E^\circ + \frac{RT}{F} \ln pO_2 + \frac{RT}{F} pO_2$	28·442	−1·233
13	$O^{=} + 1e = O_2^{2-}$	$E = E^\circ - \frac{RT}{F} \ln [O_2^{2-}] - \frac{RT}{F} pO^{=}$	40·898	−1·773
14	$2NO_3^- + 1e = 2NO_2^- + O^{=}$	$E = E^\circ - \frac{RT}{F} \ln \frac{[NO_3^-]^2}{[NO_2^-]^2} + \frac{RT}{F} pO^{=}$	67·194	−2·91
15	$2NO_3^- + 2e = 2NO_2^- + O_2^{2-}$	$E = E^\circ + \frac{RT}{2F} \ln \frac{[NO_3^-]^2}{[NO_2^-]^2} - \frac{RT}{2F} \ln [O_2^{2-}]$	108·092	−2·34
16	$NO_3^- + 2e = NO_2^- + O^{2-}$	$E = E^\circ + \frac{RT}{2F} \ln \frac{[NO_3^-]}{[NO_2^-]} - \frac{RT}{2F} \ln [O^{2-}]$	110·155	−2·388
17	$NO_2 + 1e = NO_2^-$	$E = E^\circ + \frac{RT}{F} \ln \frac{P_{NO_2}}{[NO_2^-]}$	19·376	−0·825
18	$2O^{=} + 2Cu^+ + 3NO_2^-$ $= Cu_2O + 3NO_3^-$	$pO^{=} = \frac{(\Delta G^\circ - RT \ln\{[Cu^+]^4[NO_2^-]^3/[NO_3^-]^3\})}{RT}$	−93·599	$pO^{=} = 20·5$
19	$2O^{=} + Cu^{2+} + 3NO_2^-$ $= CuO + 3NO_3^-$	$pO_2^- = \frac{-(\Delta G^\circ - RT \ln\{[Cu^{2+}][NO_2^-]^3/[NO_3^-]^3\})}{RT}$	−105·745	$pO^{=} = 23·19$

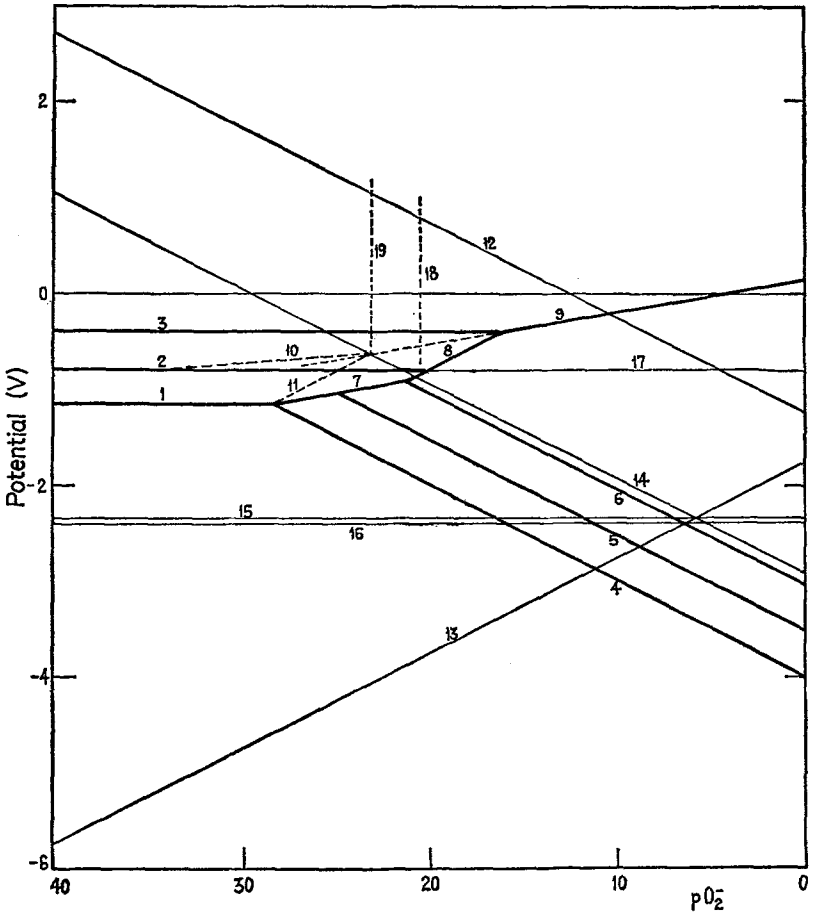

Fig. 3. Potential/pO_2^- diagram at 500K. The numbers correspond to the equilibria shown in Table 2.

with respect to the reversible nitrate electrode was taken equal to 19·37 Kcal mol^{-1} [15].

Another way to arrive at a potential/pO_2^- diagram is by a direct transformation of the potential/pO^{2-} diagram, after expressing the Nernst equations of the latter as a function of the O_2^- ion concentration derived from equilibrium in Equation 5. The Nernst equations, as expressed in terms of O_2^- ion concentration, are plotted in the potential/pO_2^- diagram shown in Fig. 4.

Similarly, a potential/pO_2^{2-} diagram (Fig. 5) can also be drawn by taking into account equilibrium Equation 9.

3. Interpretation and discussion

The thermodynamic diagrams shown in Figs. 1 to 5 comprise different areas related to the stability of metallic copper (immunity), the stability of ionic species (corrosion, active dissolution), the stability of copper oxide (passivity) and the dissolution of copper oxide (transpassivity) in the molten potassium nitrate. These regions are schematically depicted in Fig. 6.

In the potential/pO^{2-} diagram the immunity region observed at negative potentials is determined by the equilibrium lines of the Cu^+/Cu and the $Cu_2O/Cu,O^{2-}$ couples. The Cu_2O stability region is delineated by the equilibrium lines of the $Cu_2O/Cu,O^{2-}$ and $CuO/Cu,O^{2-}$ couples and the equilibrium lines of the $Cu^+,O^{2-}/Cu_2O$ system. At low pO^{2-} values and high anodic potentials the CuO stability region is observed. The boundaries of these regions are the equilibrium lines corresponding to the CuO/Cu_2O, O^{2-}, O^{2-}/O_2, $CuO/Cu^+,O^{2-}$ and CuO/Cu^{2+}, O^{2-} couples. The transpassivity region extends

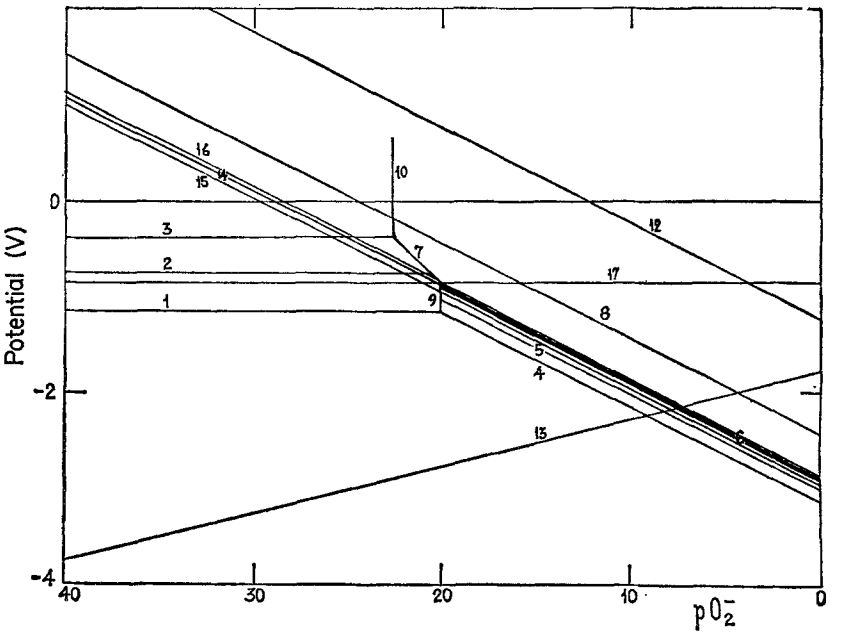

Fig. 4. Potential/pO_2^- diagram at 500K. Lines numbered 1 to 10 correspond to the Nernst equations of equilibria 1 to 10 in Table 1; lines numbered 12 to 17 correspond to the Nernst equations of equilibria 12 to 17 in Table 2. The Nernst equations are given in terms of pO_2^- taking into account equilibria of Equations 5 and 9.

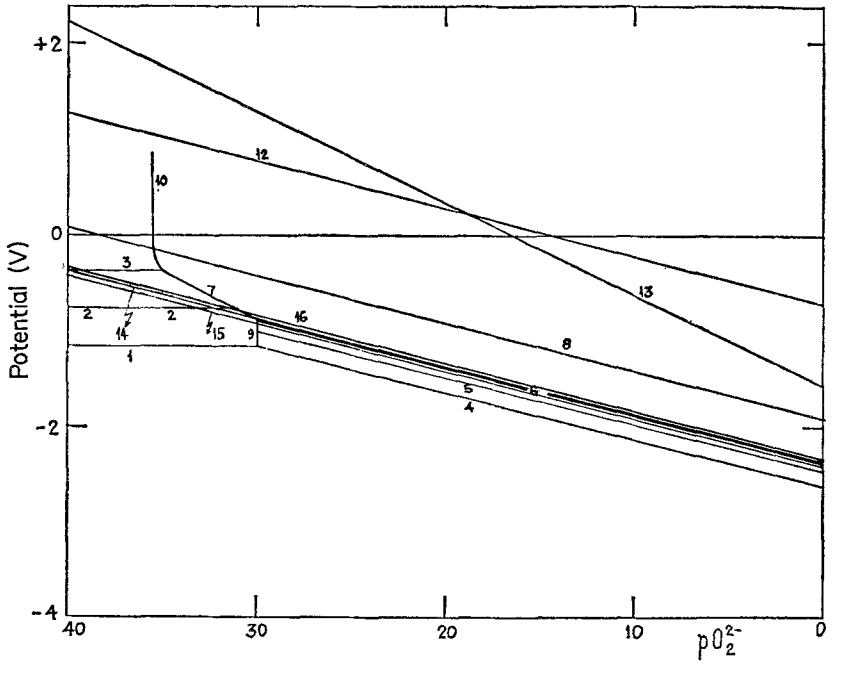

Fig. 5. Potential/pO^{2-} diagram at 500K. Lines numbered 1 to 10 correspond to the Nernst equations of equilibria 1 to 10 in Table 1; lines numbered 12 to 16 correspond to the Nernst equations of equilibria 12 to 16 in Table 2. The Nernst equations are given in terms of pO_2^{2-} taking into account equilibria in Equations 5 and9.

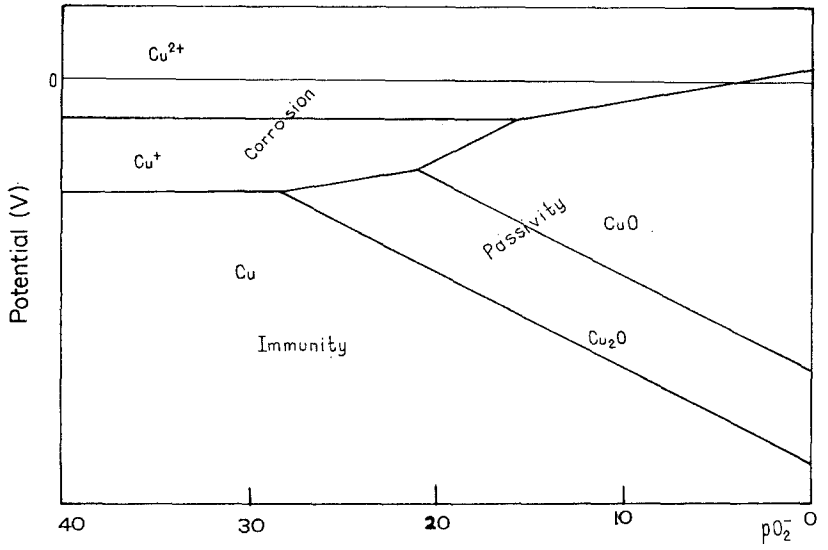

Fig. 6. Scheme of the different regions established in the potential/pO_2^- diagram.

from the O^{2-}/O_2 line upwards. At low O^{2-} ion concentration the region of active dissolution exists at potentials more anodic than approximately $-1{\cdot}0$ V. The potential/pO^{2-} diagram of molten potassium nitrate and the redox reactions at equilibrium, involving the corresponding decomposition products, has been reported earlier [2–4].

The potential/pO_2^- diagram, shown in Fig. 3, although involving an uncertainty larger than the potential/pO^{2-} diagram as a result of taking the half-wave potential of the O_2/O_2^- couple as the standard potential, gives interesting information about the copper/molten potassium nitrate system. The immunity region observed at negative potentials is determined by the equilibrium lines of the Cu^+/Cu and the $Cu_2O/Cu,O_2^-$ couples. On increasing the potential, at a low pO_2^- value, the equilibrium related to the $CuO/Cu_2O,O_2^-$ system is firstly attained and then, at higher potentials, the region corresponding to the stability of CuO is reached. But when the $Cu^{2+},O_2^-/CuO$ equilibrium line is exceeded the dissolution of the metal through the CuO passivating layer should occur with the simultaneous precipitation of CuO into the melt, as is also suggested in the transpassivity region of the potential/pO^{2-} diagram. The region delineated by the $Cu_2O/Cu,O_2^-$ and $Cu^{2+},O_2^-/CuO$ lines corresponds to metal passivation. At high pO_2^- values and at anodic potentials higher than that of the Cu^+/Cu equilibrium, the metal dissolution region is found. At pO_2^- between approximately 16 and 34, at unitary activity of the Cu^+ and Cu^{2+} ions, in the potential range between $-1{\cdot}2$ to 0·4 V, the enclosed areas correspond to a hypothetical system where equilibrium of species Cu_2O, Cu^+, O_2^-, Cu, CuO and Cu^{2+} would exist. The dashed lines drawn in the potential/pO_2^- diagram correspond to hypothetical systems. They give only an indication of the trends of the metal behaviour at equilibrium in the nitrate melt. One interesting feature of the potential/pO_2^- diagram is the existence of a rather restricted region, where copper passivation by CuO becomes possible.

On the other hand, the potential/pO_2^- diagram shown in Fig. 4 is simpler than the one shown in Fig. 3. The equilibria involved in this figure are the same as those already discussed for the potential/pO_2^- diagram. A good definition of the various regions related to the electrochemical behaviour of copper in molten nitrate is exhibited.

Similar comments apply to the potential/pO_2^{2-} diagram shown in Fig. 5. This diagram also contains a relatively large range of potential corresponding to the CuO stability, but the active dissolution region is constrained to a narrow region of potential and pO_2^{2-}.

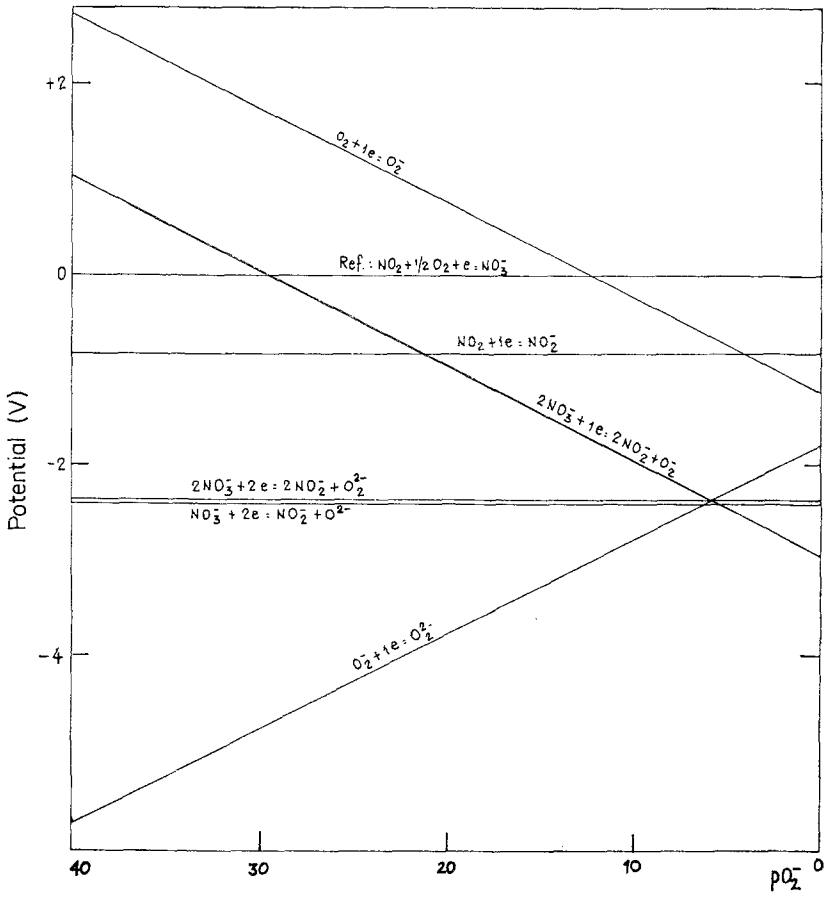

Fig. 7. Potential/pO_2^- diagram at 500K involving different equilibria with molten potassium nitrate and related products.

The potential/pO_2^- diagram corresponding to the decomposition of the melt is given in Fig. 7 to illustrate the stability regions of the melt.

Most of the features corresponding to the diagrams just described will be correlated with experimental results obtained by running current/potential voltammometric curves with copper electrodes in $NaNO_3$-KNO_3 eutectic. These results will be reported in a future publication [8].

Acknowledgement

This work is a part of the research programme of the Electrochemistry Division of INIFTA, sponsored by CONICET, UNLP and CIC (Bs.As). Professor S. L. Marchiano acted as a Faculty member of the Chemical Engineering Department of the Engineering Faculty (UNLP).

References

[1] R. N. Kunst and F. R. Duke, *J. Am. Chem. Soc.*, **85** (1963) 3338.
[2] S. L. Marchiano and A. J. Arvia, *Electrochim. Acta*, **17** (1972) 25.
[3] S. L. Marchiano and A. J. Arvia, *Electrochim. Acta*, **17** (1972) 861.
[4] A. Conte y S. Casadio, *Ric. Sci. Ital.* **36** (1966) 488.
[5] L. E. Topol, R. A. Osteryoung and J. H. Christie, *J. Phys. Chem.*, **70** (1966) 2857.
[6] P. G. Zambonin and J. Jordan, *J. Amer. Chem. Soc.*, **89** (1967) 6365; *ibid* **91** (1969) 2225.
[7] A. J. Arvia, S. L. Marchiano and J. L. San Martin, in preparation.
[8] A. Conte, *Electrochim. Acta* **11** (1966) 1579.
[9] M. Pourbaix, 'Atlas of Electrochemical Equilibria in Aqueous Solutions', Pergamon, Oxford (1966).
[10] 'Selected Values of Chemical Thermodynamic Properties', National Bureau of Standards, Circular 500, Washington (1952).
[11] K. K. Kelly, 'Contribution to the Data on Theoretical Metallurgy. XIII—High Temperature Heat Content, Heat Capacity and Entropy Data for the

Elements and Inorganic Compounds', Bull. 584, Bureau of Mines, Washington (1960).
[12] S. O. Kubaschenski and E. L. Evans, 'Metallurgical Thermochemistry', Pergamon, Oxford (1958).
[13] P. G. Zambonin, *J. Electroanal. Chem.*, **24** (1970) 365.
[14] J. Jordan, W. B. McCarthy and P. G. Zambonin, 'Characterization and Analysis in Molten Salts', G. Mamantour, Ed., M. Dekker. New York (1969).
[15] A. J. Calandra and A. J. Arvia, *Electrochim. Acta* **12** (1967) 95.